SANDIA REPORT
SAND2018-2358
Unlimited Release
Printed March 2018

Directional Unfolded Source Term (DUST) for Compton Cameras

D. J. Mitchell, S. M. Horne, S. O'Brien, and G. G. Thoreson

Prepared by
Sandia National Laboratories
Albuquerque, New Mexico 87185 and Livermore, California 94550

Sandia National Laboratories is a multimission laboratory managed and operated by National Technology and Engineering Solutions of Sandia, LLC, a wholly owned subsidiary of Honeywell International, Inc., for the U.S. Department of Energy's National Nuclear Security Administration under contract DE-NA0003525.

Issued by Sandia National Laboratories, operated for the United States Department of Energy by National Technology and Engineering Solutions of Sandia, LLC.

Available to DOE and DOE contractors from
U.S. Department of Energy
Office of Scientific and Technical Information
P.O. Box 62
Oak Ridge, TN 37831

Telephone: (865) 576-8401
Facsimile: (865) 576-5728
E-Mail: reports@osti.gov
Online ordering: http://www.osti.gov/scitech

Available to the public from
U.S. Department of Commerce
National Technical Information Service
5301 Shawnee Rd
Alexandria, VA 22312

Telephone: (800) 553-6847
Facsimile: (703) 605-6900
E-Mail: orders@ntis.gov
Online order: https://classic.ntis.gov/help/order-methods/

SAND2018-2358
Printed March 2018
Unlimited Release

Directional Unfolded Source Term (DUST) for Compton Cameras

D. J. Mitchell, S. M. Horne, S. O'Brien, and G. G. Thoreson
WMD Detect & Threat Analysis, Org. 6634
Sandia National Laboratories
P. O. Box 5800
Albuquerque, New Mexico 87185-MS0782

Abstract

A Directional Unfolded Source Term (DUST) algorithm was developed to enable improved spectral analysis capabilities using data collected by Compton cameras. Achieving this objective required modification of the detector response function in the Gamma Detector Response and Analysis Software (GADRAS). Experimental data that were collected in support of this work include measurements of calibration sources at a range of separation distances and cylindrical depleted uranium castings.

ACKNOWLEDGMENTS

This work was funded by the Department of Energy (DOE), National Nuclear Security Administration (NNSA), Org. NA-22. The assistance of Zhong He and Jiyang Chu of the University of Michigan and Jason Jaworski and Willy Kaye of H3D, Inc. is appreciated. The authors also extend their appreciation to the Defense Threat Reduction Agency (DTRA), from whom we borrowed a Polaris detector for use during this investigation. The authors also thank Klaus Ziock of Oak Ridge National Laboratory (ORNL) for assistance with collection of experimental data and advice regarding processing of data collected by imaging sensors in general.

TABLE OF CONTENTS

1. Introduction 8
2. Imager and Detector Response Function 9
   2.1. Polaris Imager 9
   2.2. GADRAS Detector Response Function 9
3. Experimental Procedure 11
4. Directional Unfolded Source Term Analysis Algorithm 14
   4.1. Computational Challenge 14
   4.2. DUST Concept 16
   4.3. Multi-Step Process 17
      4.3.1. Generate Contours 17
      4.3.2. Solve for Foreground and Background Components 17
      4.3.3. Solve for Source Terms in Contour Regions 18
      4.3.4. Adjust Individual Pixel Intensities 19
5. Results and Discussion 20
   5.1. Comparison with Other Algorithms 20
   5.2. Manual Selection of Spatial Contours 22
6. Conclusions 23
7. References 24

FIGURES

Figure 1. Configuration of CZT crystals in Polaris Versions V2.0 and V2.1. 9
Figure 2. Back-projection spectra measured by Polaris Version 2.1 (dots) are compared with calculations (lines) for three angular groups. 11
Figure 3. A gamma-ray image of the ^{133}Ba source (red fading to blue) is superimposed over an optical image recorded by Polaris while calibration sources were separated by ±20 cm in vertical and horizontal directions. 12
Figure 4. This optical image shows the 18-kg DU casting on the left and the 9-kg DU casting on the right. The spacing between the DU castings is 25 cm. 14
Figure 5. Measured back-projection spectra for ^{137}Cs in several angular groups are compared after dividing the count rates by the solid angles associated with the acceptance angles. 15
Figure 6. The SBP image for FourSources-10cm is displayed on the left and spectra associated with the three quadrants containing observable sources is shown on the right. Both of these images use red, green, and blue to signify ^{133}Ba, ^{137}Cs, and ^{60}Co, respectively. 16
Figure 7. The contours that were generated by the automatic method applied to FourSources-10cm are displayed in this image. 17
Figure 8. Measured foreground and background spectra derived from the SBP data cube is compared with computed continua. 18
Figure 9. Source terms computed by DUST are displayed for the three spatial groups. 19

Figure 10. The source image and source terms in three spatial regions computed by DUST for FourSources-10cm are displayed in this figure.....20
Figure 11. The source image and spectra in three spatial locations computed by FBP for FourSources-10cm are displayed in this figure.....21
Figure 12. The total foreground source term computed by DUST for the FourSources-10cm measurement (black error bars) are compared with computed spectra for the three radionuclides returned by the isotope identification algorithm.....21
Figure 13. The left side of the figure shows the SBP image and right side shows an optical image of the polyethylene sphere containing a ^{137}Cs source. 22
Figure 14. The left side shows the DUST image and the graph to the right displays the source terms for the central region (green) and outer annular region (red).....23

TABLES

Table 1. Source Displacements and Angular Separations 13
Table 2. Calibration Sources Used During the ORNL Measurements 13
Table 3. Color Codes for Display of Gamma-ray Images 15

NOMENCLATURE

Abbreviation	Definition
CC	Compton Camera
CZT	Cadmium Zinc Telluride
DLL	Dynamic-link Library
DP	Depleted Uranium
DRF	Detector Response Function
DTRA	Defense Threat Reduction Agency
DUST	Directional Unfolded Source Term
EIID	Energy Imaging Integrated Deconvolution
FBP	Filtered Back Projection
GADRAS	Gamma Detector Response and Analysis Software
GeGI	Germanium Gamma Imager
ORNL	Oak Ridge National Laboratory
SBP	Simple Back Projection
UM	University of Michigan
χ_r^2	Reduced chi-square difference

1. INTRODUCTION

Compton cameras (CC) are position-sensitive detectors that image gamma-ray sources by examining energies and positions of coincident photon interactions. The angular deflection of the scattered photon with respect to the incident gamma ray is a function of the energies of the incident and scattered gamma rays as defined by the Compton-scatter relationship [1]. Although the calculation is fundamentally simple, doing so requires measurement of the energies of each interaction, and the final interaction must be a photoelectric event, which deposits the full energy of the scatted photon within the detector. The origin of the incident gamma ray is constrained to a conical region defined by the angular deflection and vector of the scattered photon. Spatial probability distributions can be constructed by recording numerous interactions. Since the incident gamma-ray energies are determined for each event, the spatial distributions can be tallied as a function of incident gamma-ray energy. The multi-dimensional probability distribution is referred to as a Simple Back Projection (SBP). The SBP spectra and images are inherently indistinct because probability distributions are constructed from conical projections that define regions where sources may be located rather than specific coordinates. Additional blurring of the reconstructed images and spectra is attributable to several factors, including: the scattered photons may exit the detector before depositing the full energy; uncertainties in energies of the discrete events broaden the probability cones; and the detector may not resolve multiple scatter events that occur in close proximity. Methods have been developed that improve the sharpness of CC images [2] [3] [4], but the solutions may be non-unique, particularly if the data have poor statistical quality or radiation sources are spatially distributed.

The majority of research pertaining to Compton cameras has been directed toward the goal of improving the image quality. The effort described in this paper emphasizes spectral analysis, so instead of just representing radiation intensity profiles, we seek to improve the ability to perform assessments, such as mapping activity contours for specific radionuclides. Directionally resolved spectra also provides additional constraints that can be used to construct models for macroscopic sources, which is often referred to as solving the inverse problem [5] [6].* This capability can be applied to a variety of applications, including: nuclear emergency response, medical imaging, and arms control treaty verification [7]. Our approach applies a Detector Response Function (DRF) that represents the response of a detector as a function of the energy of incident gamma rays and the angle between the SBP spatial element and the actual source location. The DRF is an extension of the Gamma Detector Response and Analysis Software (GADRAS) [8], which only supported nondirectional detectors prior to development reported in this document. The algorithm developed to process data collected by Compton cameras computes what we call the Directional Unfolded Source Term (DUST), which describes the surface leakage spectrum in units of photons per second for each spatial element. The processing method described in this paper should apply to any Compton camera, but results that are presented here pertain specifically to the Polaris Version 2.1 imager, which was manufactured and developed jointly by H3D, Inc. and LocoLabs.

* The objective of the forward problem is to compute the response of a detector to a known source.

2. IMAGER AND DETECTOR RESPONSE FUNCTION

2.1. Polaris Imager

Polaris is a gamma-ray imager that can be operated as a Compton camera, a coded aperture imager, or a non-directional gamma-ray spectrometer. This paper only addresses the use of the instrument as a Compton camera. Polaris incorporates 18, 2 cm×2 cm×1.5 cm CZT detectors that are stacked in two planes. Figure 11 shows the arrangement of crystals in V2.0 and V2.1 Polaris systems. The use of pixelated CZT crystals and analog electronics provides a lateral pixel resolution of 1.7 mm and a depth resolution of 0.5 mm. List-mode files that are recorded by the instrument are post-processed by a dynamic-link library (DLL) provided by H3D to generate SBP data cubes with 2-degree resolution. We retain the convention established by H3D, where $\theta = 0°$ corresponds to polar north (directly overhead) and the location that is normal to the detector plane corresponds to $(\phi,\theta) = (90°,90°)$, which is the center of the field of view for measurements reported in this paper.

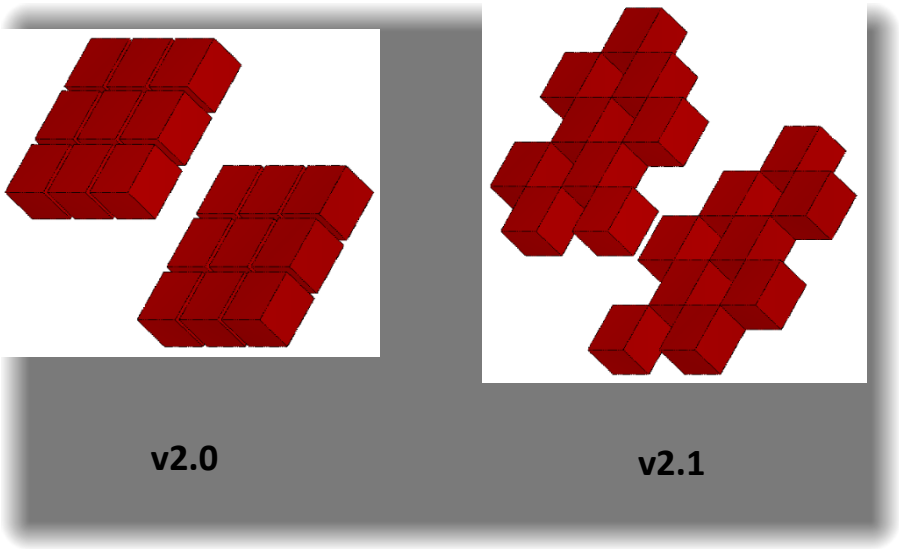

Figure 1. Configuration of CZT crystals in Polaris Versions V2.0 and V2.1.

2.2. GADRAS Detector Response Function

GADRAS applies an analytic response function to compute photopeak probabilities, radiation continua resulting from gamma rays that scatter out of detectors, and other features such as escape peaks. The chemical composition of the detector material defines cross sections for photoelectric absorption, Compton scatter, and pair production. Continua associated with radiation that scatters into detectors are computed by interpolating a pre-computed library[†] of environmental scatter calculations, then adding an analytic representation of continua derived from local scattering, which occurs within detector housings. Empirical parameters that define these characteristics are adjusted so that computed spectra match measurements for a series of

[†] MCNP was used to compute the scatter library.

calibration sources. This approach enables calculation of the gamma-ray detector response in under one second for non-imaging sensors.

The geometric configuration of all the detector elements in an imaging sensor could be represented explicitly and the response could be computed by Monte Carlo methods, but doing so is computationally intensive. While inspecting characterization measurements, we observed that the responses of Polaris Versions 2.0 and 2.1 are similar despite substantial differences in their configurations (see Figure 1), which suggested that explicit representation of the detector configuration may not be required. Accordingly, the approach that we pursued was to apply empirical parameters to represent characteristics that are associated with Compton cameras in a probabilistic way. In addition to the parameters that are normally applied to characterize non-directional sensors, the modified response function applies the following CC parameters:

- *Spatial Coverage* is the percent of space that is intercepted by other detector elements,
- *Correct Pixel* is the percent of events that are scored in the correct spatial element,
- *Angular Resolution* is the angular resolution in degrees.

The subroutine that GADRAS uses to compute spectra for non-imaging detectors was modified to synthesize back-projection spectra. Imageable events require that at least two interactions within the detector, so photoelectric absorption of the incident gamma-ray or interactions where the initial recoil photon escapes the array are not tallied. Events for which the scattered photon is absorbed on the second or third interaction are scored in the accrued photopeak probability. The photopeak probability is greatest in the direction where the source is located, but photopeaks are also attributed to other spatial regions because of the indistinct nature of the probability cones as described by the *Correct Pixel* parameter. Events associated with incomplete absorption of scattered photons following two or more interactions contribute to continua that are diffuse in both energy and spatial locations.

Our first approach was to apply the exact dimensions of individual CZT crystals and a scalar of 18 to represent the fact that the complete assembly contains 18 detector elements. The three CC parameters plus attenuation and scatter parameters were adjusted to fit measurements for several calibration sources. This approach yielded a reasonable approximation (generally within a factor of two) of the detector response, but a perfect match could not be obtained for the multi-dimensional problem of matching photopeaks and continua as a function of both the incident gamma-ray energy and the spatial location with respect to the actual source location. Therefore, an alternative approach was explored, where the detector was represented as a large number of elements with volumes of approximately 1 mm^3, which corresponds to the pixel resolution for the Polaris detector. The accuracy of the fit was similar after adjusting the empirical parameters. Since neither description was clearly superior, we elected to apply the first approach because asserting the exact dimensions and number of the CZT crystals and only adjusting the parameters that are fundamentally empirical was more grounded in physical attributes.

It was apparent that the accuracy of the multi-dimensional response function was compromised by numerous approximations that were made in order perform the calculations quickly. The problem was addressed by applying empirical adjustments to correct the analytic solution described above. The adjustments define scalars for photopeak and continua intensities as a function of gamma-ray energies and angle between the spatial element and the actual source location. This approach is not as convenient as the characterization process for non-imaging detectors because the empirical scalars must be adjusted for each detector configuration,[‡] but the

resulting accuracy is as comparable to what can be achieved for non-imaging detectors. Figure 2 illustrates the agreement between computed spectra and measurements that was achieved for a ^{60}Co source at three ranges of angular separation, δ, between the spatial elements in the data cube and the actual source location. Comparable accuracy was also achieved for ^{133}Ba, ^{137}Cs, and ^{232}U sources. The region below 200 keV is displayed with gray background because this region is not weighted when calculations are performed.

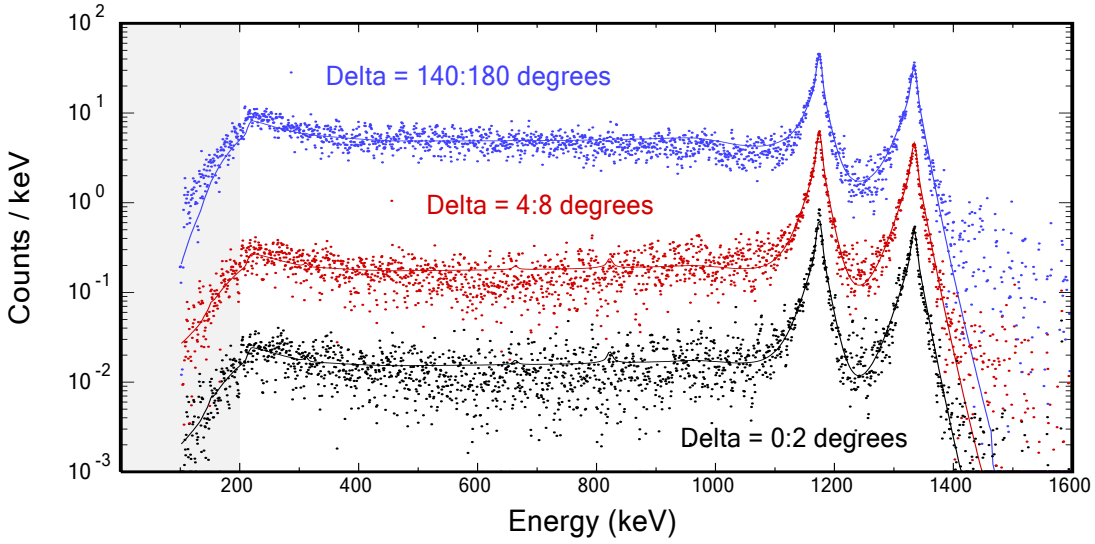

Figure 2. Back-projection spectra measured by Polaris Version 2.1 (dots) are compared with calculations (lines) for three angular groups.

3. EXPERIMENTAL PROCEDURE

A series of measurements were performed at Oak Ridge National Laboratory (ORNL) using a Polaris V2.1 sensor.[§] The sensor was placed on a table 100 cm from a low-mass stand to which calibration sources were attached. The sources were positioned in a planar grid where each source was displaced by the same amount in the vertical and horizontal directions relative to the central point. Table 1 lists the displacements and the corresponding angular separations between the closest sources. Figure 3 shows an optical image recorded by Polaris with sources displaced by 20 cm in vertical and horizontal directions relative to the center of the array. The overlay in the upper-left quadrant represents emission from a ^{133}Ba source as determined by the H3D processing software. The object at the center of the field of view on the far side of the calibration source array is a Germanium Gamma Imager (GeGI), which also recorded image spectra while these measurements were performed. Table 2 lists activities of the calibration sources at the time the measurements were performed. Measurement durations were approximately one hour.

[‡] Different empirical adjustments are applied for Polaris V2.0 and V2.1.

[§] Measurements were also performed using a GeGI detector and coded aperture reconstruction software that was developed at ORNL, but these results are not reported in this document.

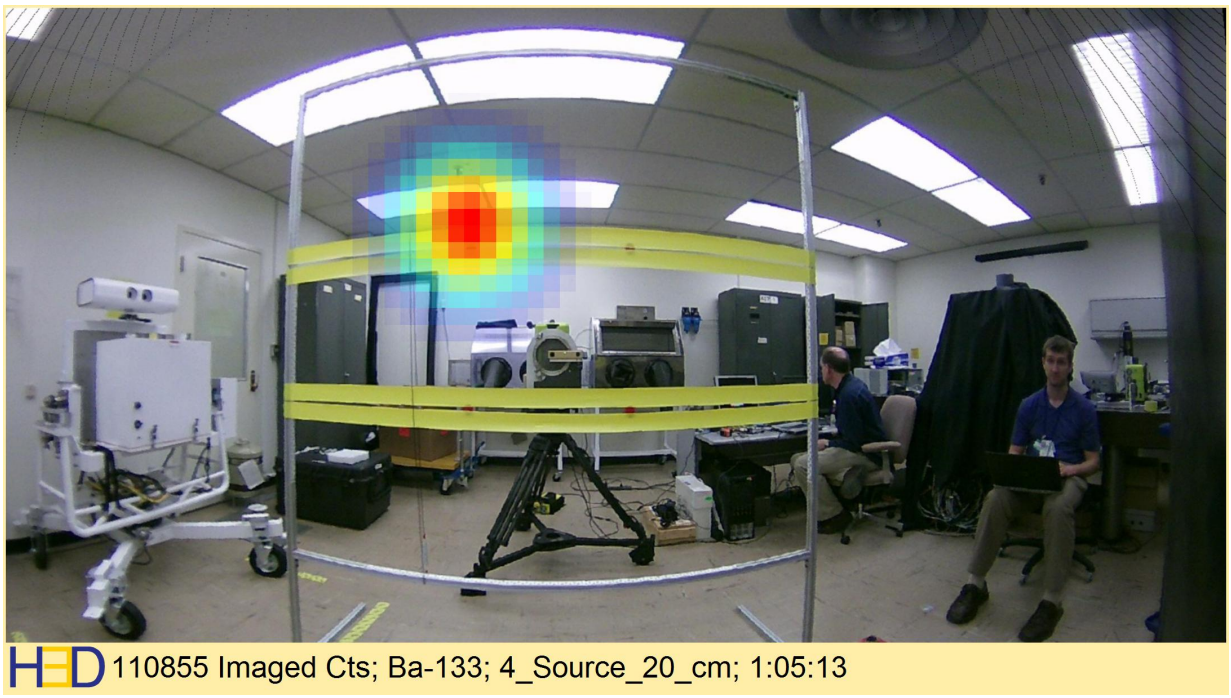

Figure 3. A gamma-ray image of the ^{133}Ba source (red fading to blue) is superimposed over an optical image recorded by Polaris while calibration sources were separated by ±20 cm in vertical and horizontal directions.

Table 1. Source Displacements and Angular Separations

Source Displacements (cm) in Vertical and Horizontal Directions Relative to the Center	Angular Separation Between Closest Sources (degrees)
1	1.1
2	2.3
5	5.7
10	11.4
15	17.1
20	22.6
30	33.4
50	53.1

Table 2. Calibration Sources Used During the ORNL Measurements

Radionuclide	Activity (μCi)
^{241}Am	106.3
^{133}Ba	65.5
^{137}Cs	82.9
^{60}Co	38.3

In addition to measurements of calibration sources, which are effectively point sources, measurements were also performed for depleted uranium (DU) castings. The DU castings present a different type of challenge because the emission is distributed both spatially and in energy due to the Bremsstrahlung continua. Figure 4 shows a configuration with an 18-kg, cylindrical DU casting on the left (13 cm OD, 15 cm long) and a 9-kg DU casting on the right (13 cm OD, 7.5 cm long).

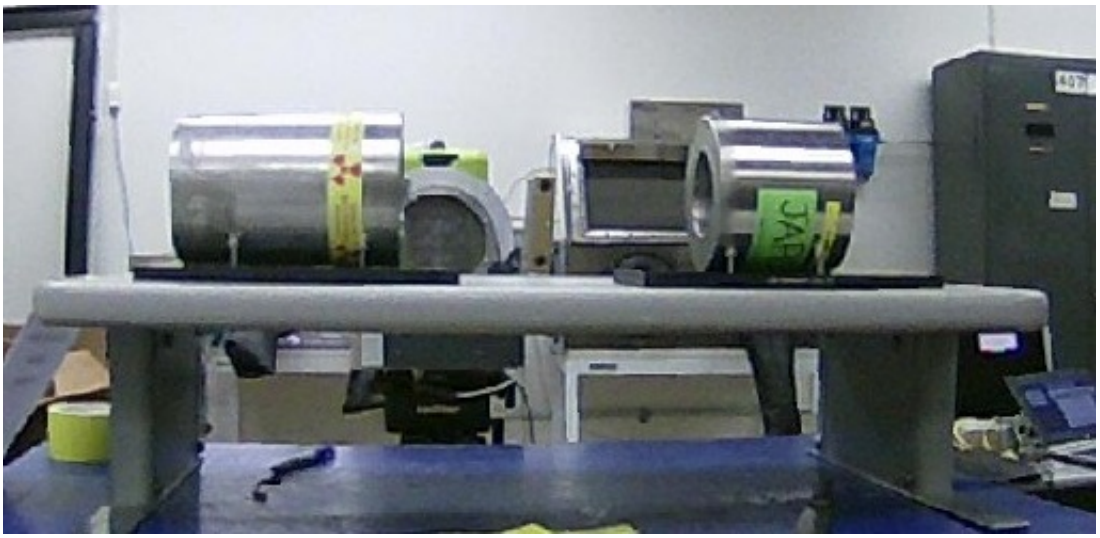

Figure 4. This optical image shows the 18-kg DU casting on the left and the 9-kg DU casting on the right. The spacing between the DU castings is 25 cm.

4. DIRECTIONAL UNFOLDED SOURCE TERM ANALYSIS ALGORITHM

4.1. Computational Challenge

Compton back-projection spectra exhibit features that vary with the angle between the spatial element and actual source location, so gamma-ray spectra can be evaluated as a function of position. However, achieving this goal is challenging because differences in back-projection spectra as a function of position are subtle. The challenge is illustrated in Figure 5, which displays SBP spectra recorded by Polaris Version 2.1 in several angular groups with respect to the actual location of a ^{137}Cs source. After scaling by the solid angle, photopeak intensities decrease with increasing difference between the source location and the angular separation of the spatial group (δ), but differences are small below about 10 degrees. The continuum intensities and shapes vary only slightly with δ except in energy regions directly below photopeaks.

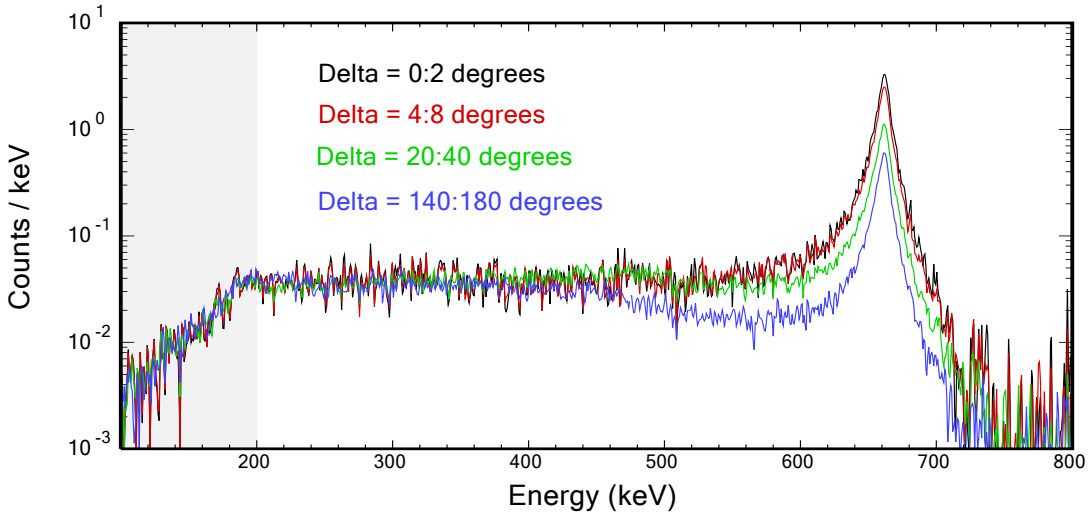

Figure 5. Measured back-projection spectra for ^{137}Cs in several angular groups are compared after dividing the count rates by the solid angles associated with the acceptance angles.

This section describes the DUST method and shows examples of how this approach is applied to processing measurements of the four calibration sources at separation of ±10 cm relative to the common center. This configuration is referred to as *FourSources-10cm*. The array of calibration sources includes ^{241}Am, but the energy of the primary gamma-ray (60 keV) is too low to be observed by Polaris in Compton camera mode. Therefore, gamma rays are only observed for ^{133}Ba, ^{137}Cs, and ^{60}Co, which are located in the upper-left, the lower-right, and the lower-left quadrants, respectively. The SBP image and plots of spectra for spatial regions associated with the three observable calibration sources are displayed in Figure 6. The following color codes are used to represent gamma-ray images in this and subsequent plots:

Table 3. Color Codes for Display of Gamma-ray Images

Color	Energy range (keV)
red	250 to 450
green	450 to 700
blue	700 to 2700

The same color codes are used to associate spectra with spatial regions to which they correspond.

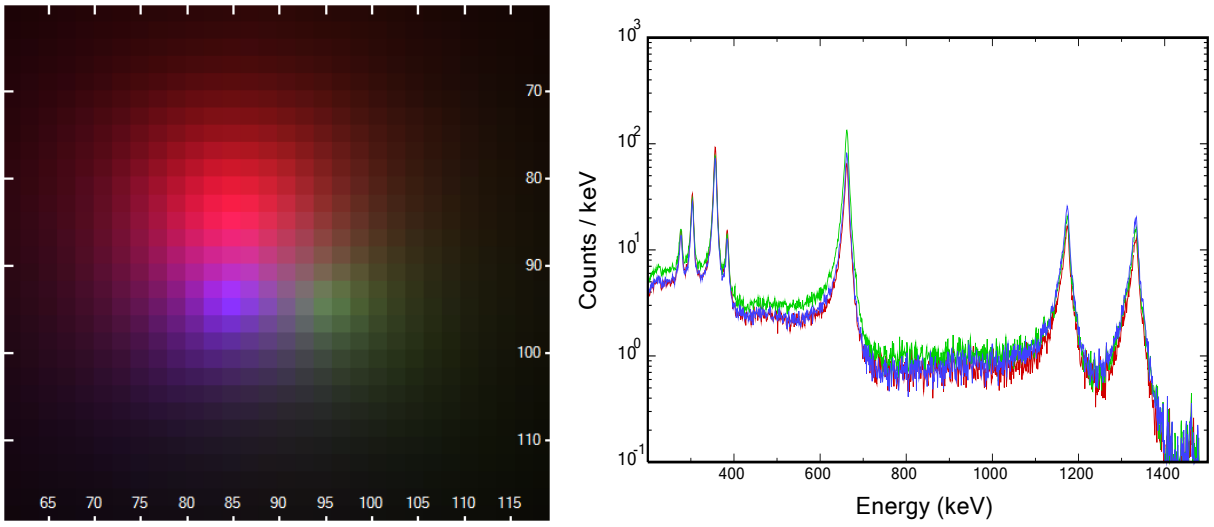

Figure 6. The SBP image for *FourSources-10cm* is displayed on the left and spectra associated with the three quadrants containing observable sources is shown on the right. Both of these images use red, green, and blue to signify ^{133}Ba, ^{137}Cs, and ^{60}Co, respectively.

4.2. DUST Concept

The objective of the Directional Unfolded Source Term (DUST) analysis method is to process SBP data cubes to extract spectroscopically accurate gamma-ray source profiles as a function of spatial location. The process is conceptually straightforward: solve for source terms starting with the highest energy group; strip the estimated continuum from lower-energy groups; repeat the process for decreasing energy groups. The first step of this process can is represented by Eq. (1):

$$Y_{i,j} = \sum_{k=1}^{nAngles} R_{i,\delta(j,k)} S_{i,j} \tag{1}$$

where $Y_{i,j}$ is the count rate recorded in energy group i and spatial group j; $R_{1:i,\delta(j,k)}$ is the full-energy response for energy group i and angle δ between spatial groups j and k; and $S_{i,k}$ represents the source terms, in units of photons per second in energy group i and spatial group k. Equation (1) is solved by non-negative linear regression.

The second step of the process strips continua derived from the estimated source terms according to the following equation:

$$Y_{1:i-1,j} = Y_{1:i-1,j} - \sum_{k=1}^{nAngles} R_{1:i-1,\delta(j,k)} S_{i,k} \tag{2}$$

The value of i is decremented and the process is repeated for lower-energy groups. The response matrix that is interpolated when the calculations are performed applies perfect energy resolution to prevent additional broadening of the source term beyond the intrinsic resolution of the

measured spectra. The detector response $R_{1:i,\delta(j,k)}$ is averaged over the extents of the spatial groups j and k when the calculations are performed.

4.3. Multi-Step Process

In principal, the process described in Section 4.2 could be applied by processing all of the spatial source terms and energy groups as independent variables. The flaw in this approach is revealed by observing that there are 10^7 degrees of freedom if there are 1000 energy groups and 100 spatial elements in ϕ and θ directions. Accordingly, the solutions are non-unique and dominated by statistical variability. Several methods were explored to improve the spectral accuracy and to reduce uncertainties in these estimates. The best results were obtained by applying the multi-step process to estimate the source terms. The process described in Section 4.2 is applied repeatedly using different spatial and energy groupings.

4.3.1. Generate Contours

Contours can be generated by either automatic or manual procedures. The automatic procedure creates contours based on count rates in each of several energy groups. Overlapping regions are combined if the spectral characteristics are not significantly different. Figure 7 shows contours that were generated by the automatic method for *FourSources-10cm*. Contour regions represent the first pass in the identification of source locations. Unless stated otherwise, all results presented in this document apply automatic contour selections because the results are less subjective than processes that require user intervention. Manual selection can be advantageous if the visual image reveals locations of interest that are not resolved by the automatic process.

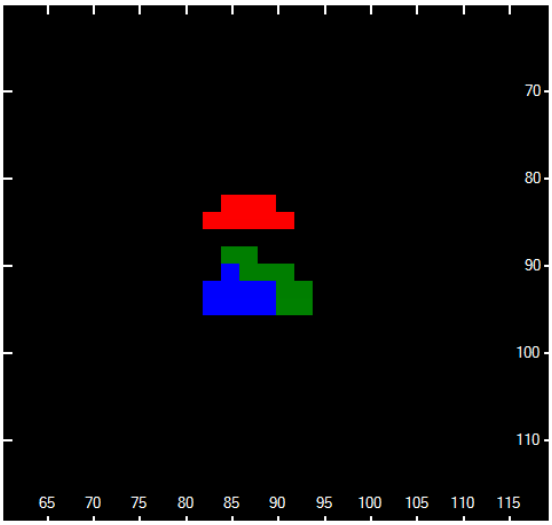

Figure 7. The contours that were generated by the automatic method applied to *FourSources-10cm* are displayed in this image.

4.3.2. Solve for Foreground and Background Components

The best statistical confidence for gamma-ray source terms is obtained by using the fewest number of spatial elements. Solving for just foreground versus background source terms without attempting to identify variations within either spatial group provides the best estimate of leakage spectra because it only uses two spatial groups. Pixels contained in all of the selected contours

are combined to represent the foreground spatial region and everything else is treated as background. Even with this minimal number spatial groups, partitioning the leakage can still create non-physical spectral characteristics. This problem is addressed by using the intensities of peaks at 1460, 1764, and 2614 keV to estimate contributions from ^{40}K, ^{226}Ra, and ^{232}Th, which are applied to synthesize a rough estimate for the source term associated with background radiation. Application of the estimated background as a loose constraint for the linear regression solution eliminates most of the artifacts that would otherwise be observed in both foreground and background source terms.

As noted in Section 4.1, spectral continua exhibit similar shapes and intensities after normalizing by the solid angles of the spatial groups, so the evaluation of the spectral continuum derived from the foreground/background solution can be applied to strip spectra in all subsequent solutions without computing the continua explicitly for every angular separation. This approximation is not essential to the execution of the DUST algorithm, but it accelerates calculations substantially. Errors that are introduced by neglecting the angular dependence of the continuum in regions immediately below photopeak energies are compensated by analytic adjustments after solving for the source terms in the spatial groups (Section 4.3.3). Figure 8 displays measured and computed components for the foreground and background spatial regions. The computed continua, which includes background radiation as well as continuum derived from the calibration sources, is used to strip spectra according to Eq. (2) in subsequent steps.

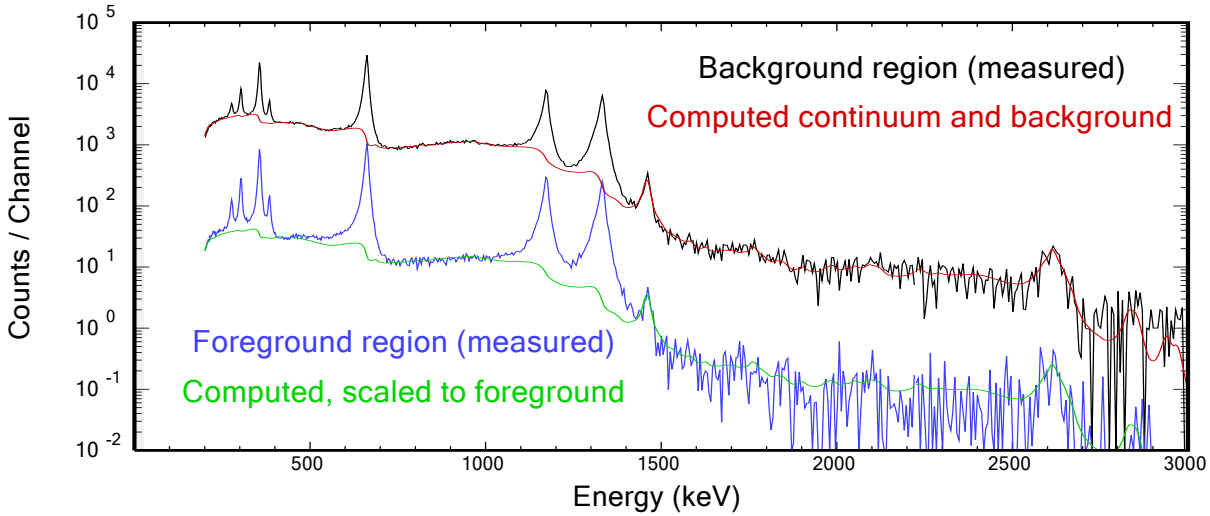

Figure 8. Measured foreground and background spectra derived from the SBP data cube is compared with computed continua.

4.3.3. Solve for Source Terms in Contour Regions

The next step of the process is to compute the average source term within each contour region. The foreground/background solution is applied by using the foreground source term to constrain the sum of the spatial source terms with 1% uncertainty. The continuum associated with background radiation and continuum derived from the foreground component is stripped as the solver progresses from high to low energy. Processing the data in this way eliminates much of the ambiguity in the solution, but gamma rays are still attributed to the wrong spatial group occasionally. This is evidenced by non-physical drop outs for source terms, like those occurring

at 650, 1200, and 1400 keV in the red curve on the left side of Figure 9. This plot corresponds to gamma-ray source terms derived by analyzing the SBP data cube for the two DU castings arranged as shown in Figure 4. The discrepancies are addressed by using non-negative regression to fit the source terms with linear combinations of templates derived from a library containing about 70 radionuclides and numerous shielding combinations. The fits to the source terms are then used to loosely constrain (100% uncertainty) the solutions and the fitting process for the source terms that are repeated. The plot on the right-side of Figure 9 shows the source terms that are obtained after applying the constraint.

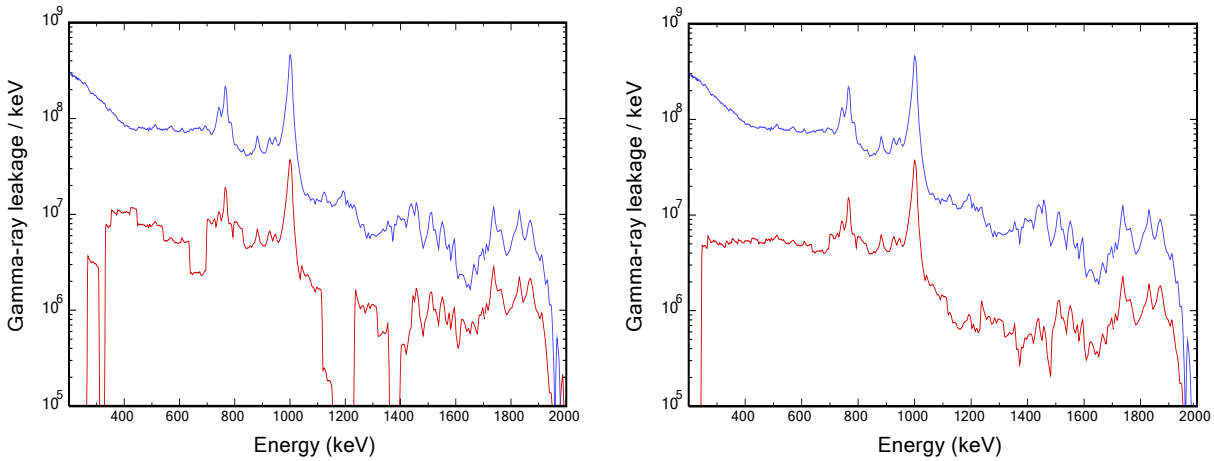

Figure 9. Source terms computed by DUST are displayed for the three spatial groups.

4.3.4. Adjust Individual Pixel Intensities

The last DUST process adjusts individual pixel intensities while retaining the total source terms computed in previous steps. Figure 10 shows the final result for the image and source terms derived by processing the SBP data cube for *FourSources-10cm.* The DUST algorithm assigns the source terms to the correct spatial groups with less than 1% spillage into other spatial groups. Note that the vertical axis displays the gamma-ray leakage, which is a substantial improvement in information content because it pertains directly to source intensity without the need for further accounting for the detector efficiency. The horizontal distribution of source intensities is a peculiarity associated with this particular measurement, and images do not generally exhibit this degree of structure.

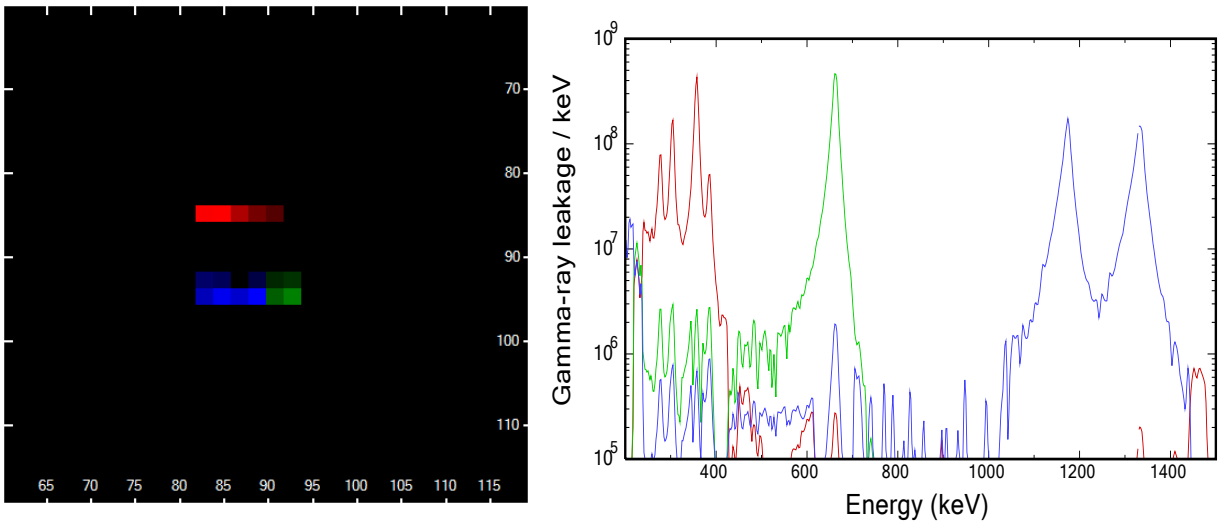

Figure 10. The source image and source terms in three spatial regions computed by DUST for *FourSources-10cm* are displayed in this figure.

5. RESULTS AND DISCUSSION

The performance of the DUST algorithm is evaluated according to several criteria. The first criterion is how it performs versus other Compton camera reconstruction methods. The second criterion is the suitability of computed source terms for spectral analysis, which requires accurate spectral shapes, magnitudes, and uncertainties. The final topic that is discussed in this section is an evaluation of automated selection of contours versus the manual method that was also developed.

5.1. Comparison with Other Algorithms

DUST analysis begins with the output of the H3D, Inc. developed SBP algorithm, so it is an analysis enhancement as opposed to being an entirely independent process. Execution of DUST is completed in several seconds, and is suitable for real-time applications. A Filtered Back Projection (FBP) method [3], developed by researchers at the Univ. of Michigan (UM), is another fast algorithm that can process data collected by Polaris. Figure 11 presents FBP results that are comparable to the DUST evaluation shown in Figure 10. The gamma-ray images differ, but the spatial resolution is an improvement over SBP in both cases, and conclusions regarding the source separations and small spatial extents are essentially the same. Differences in spectral components are more pronounced. DUST is substantially more effective in distinguishing emissions from the three closely spaced sources. Comparisons between DUST and an Energy Imaging Integrated Deconvolution (EIID) algorithm [2], which was also developed at UM, were also performed. The EIID algorithm offers some advantages with respect to image reconstruction, but directional spectra are generally less well resolved compared with DUST, and computation time is orders of magnitude longer. A companion document [9] has been prepared that compares DUST with analysis results obtained by other algorithms for all of the measurements described in Section 3.

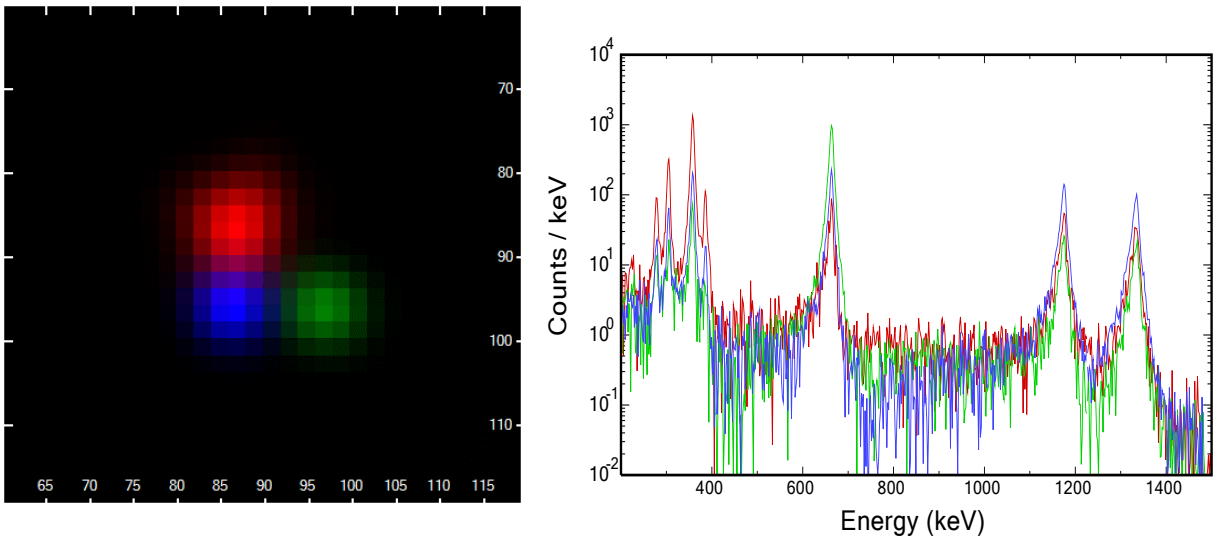

Figure 11. The source image and spectra in three spatial locations computed by FBP for *FourSources-10cm* are displayed in this figure.

5.2. Analysis Results

Spectra shown in Figure 10 display clear separation between emissions from the three radionuclides, but quantitatively spectroscopic analysis also requires accurate spectral shapes and error estimates. Figure 12 presents a graphic display of isotope identification results that are obtained when the sum of the source terms for the three spatial regions are analyzed by the HPGeFSA, which is an automated analysis algorithm that is contained in GADRAS. The relative intensities and peak shapes are in good agreement across the spectrum. The estimated activities are accurate to within about 10% after compensating for source distances.

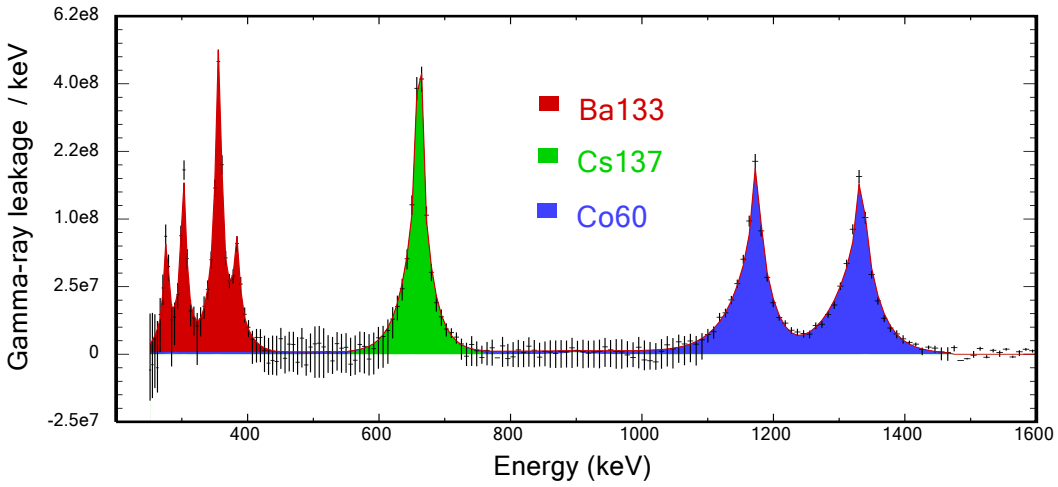

Figure 12. The total foreground source term computed by DUST for the *FourSources-10cm* measurement (black error bars) are compared with computed spectra for the three radionuclides returned by the isotope identification algorithm.

5.3. Manual Selection of Spatial Contours

An operator may have access to information, such as an optical image, that suggests spatial regions of interest that are not obvious in the SBP reconstruction. The measurement of the 83 μCi ^{137}Cs source inside a polyethylene sphere (23 cm internal diameter, 38 cm outside diameter) is an example that illustrates the advantage of the manual approach versus automated contour selection. Figure 13 shows both visible and SBP images of this test object. A question that might be asked is whether a small ^{137}Cs source is present within the polyethylene as opposed to being distributed throughout the sphere. Manual selection of contour regions allows the DUST algorithm to begin with two manually selected contours, corresponding to a few pixels where the radiation is most intense within a larger annular contour. Figure 14 shows the resulting image and spectra for the two regions. The 661-keV photopeak is clearly defined in the central region whereas the outer region is dominated by a lower-energy continuum corresponding to scattered photons. These results lead to the conclusion that the ^{137}Cs is concentrated at the center of the object, and the intensity of scattered radiation relative to un-scattered gamma rays could also be used to infer the polyethylene thickness.

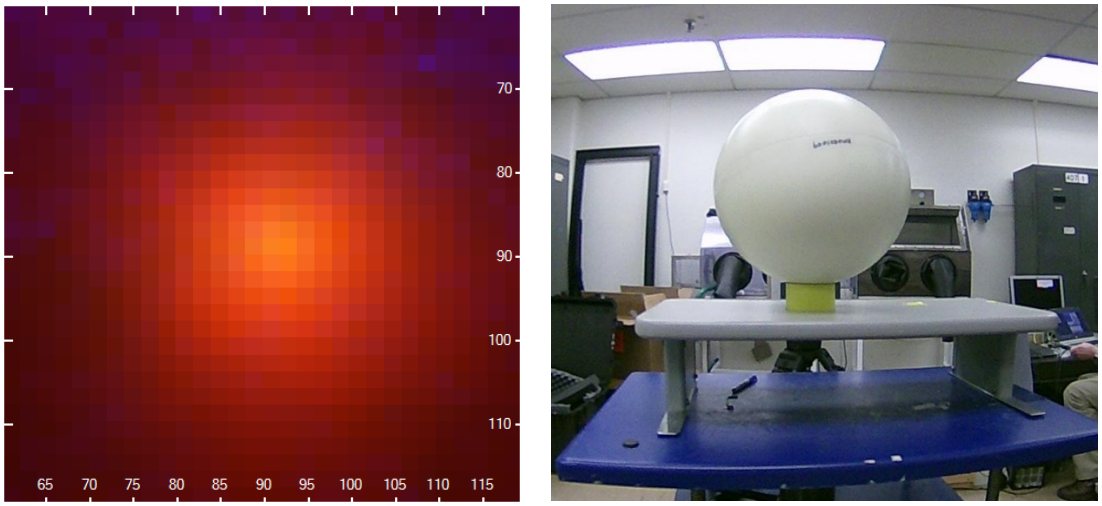

Figure 13. The left side of the figure shows the SBP image and right side shows an optical image of the polyethylene sphere containing a ^{137}Cs source.

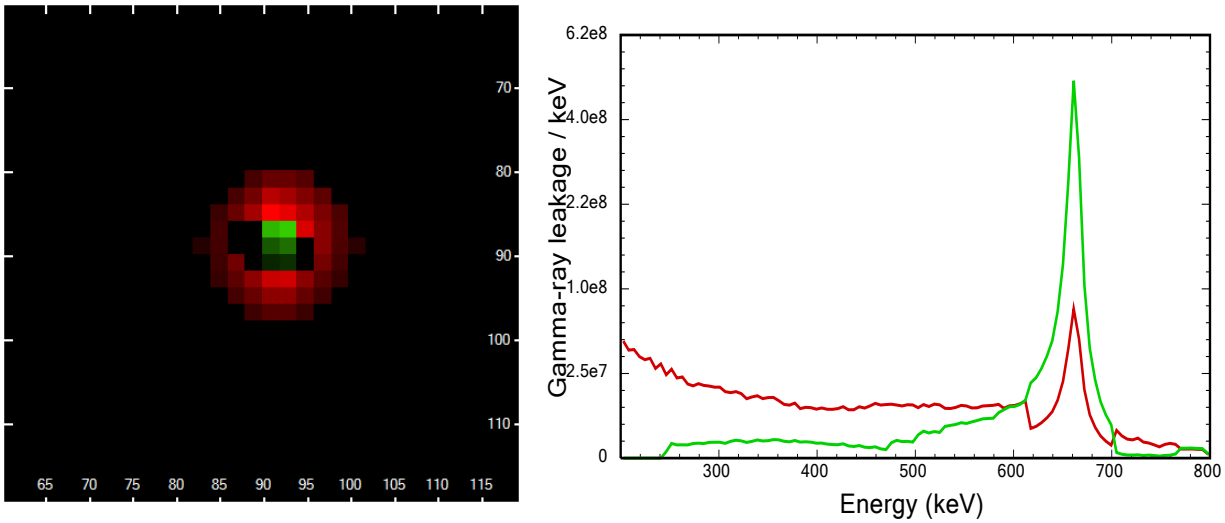

Figure 14. The left side shows the DUST image and the graph to the right displays the source terms for the central region (green) and outer annular region (red).

6. CONCLUSIONS

The DUST algorithm achieves the goal of enabling improved spectral analysis using data collected by Compton cameras. The algorithm executes quickly, it is able to partition the emission from closely spaced gamma ray sources into the correct spatial groups, and output spectra are accurate representations of the true gamma-ray source terms. The GADRAS application was modified to enable viewing and analysis of data collected by Compton cameras in a way that is analogous to non-directional gamma-ray spectrometers.

7. REFERENCES

[1] G. F. Knoll, Radiation Detection and Measurement, USA: John Wiley & Sons, Inc., 1979.

[2] D. Xu and Z. He, "Gamma-ray energy-imaging integrated spectral deconvolution," *Nuclear Instruments and Methods in Physics Research Section A: Accelerators, Spectrometers, Detectors and Associated Equipment 574, no. 1,* pp. 98-109, 2007.

[3] J. Chu, M. Streicher, J. A. Fessler and Z. He, "Unbiased Filtered Back-Projection in 4Pi Compton Imaging with 3D Position Sensitive Detectors," *IEEE Transactions on Nuclear Science, Vol. 63, No. 6,* pp. 2750-2756, 2016.

[4] W. Wang and Z. He, "Detecting Shielded Sources Using 3-D CdZnTe Detectors," *IEEE Trans. Nucl. Sci., vol. 63, no. 6,* pp. 465-467, 2016.

[5] Y. Censor, M. D. Altschuler and W. D. Powlis, "A computational solution of the inverse problem in radiation-therapy treatment planning," *Applied Mathematics and Computing, vol. 25, issue 1,* pp. 57-87, 1988.

[6] D. J. Mitchell and J. Mattingly, "A Framework for the Solution of Inverse Radiation

Transport Problems," *IEEE Nuclear Science Symposium Conference Record, N02-439,* pp. 3734-3743, 2008.

[7] A. J. Flynn, W. A. Amai, P. B. Merkle, L. F. Anderson, J. D. Strother, T. M. Weber and J. L. Etzkin, "Next Generation Trusted Radiation Identification System (NG-TRIS)," Sandia National Laboratories, Albuquerque, NM, 2010.

[8] S. M. Horne, G. G. Thoreson, L. A. Theisen, D. J. Mitchell, L. Harding and W. A. Amai, "GADRAS-DRF 18.6 User's Manual," Sandia National Laboratories Report, SAND2016-4345, 2016.

[9] S. O'Brien, D. J. Mitchell, S. M. Horne and G. G. Thoreson, "Directional Software Algorithms and Sensors Evaluation," Sandia National Laboratories Report, SAND2018-XXXX, 2018.

DISTRIBUTION

1	SNL/MS0782	Dean J. Mitchell	6634 (electronic copy)
1	SNL/MS0782	Steve M. Horne	6634 (electronic copy)
1	SNL/MS0782	Sean O'Brien	6634 (electronic copy)
1	SNL/MS0782	Gregory G. Thoreson	6634 (electronic copy)
1	SNL/MS0899	Technical Library	9536 (electronic copy)
1	DOE/NNSA/NA-22	Michael Koehl	(electronic copy)
1	DTRA	Marc Black	(electronic copy)
1	H3D Inc.	Willy Kaye	(electronic copy)
1	H3D Inc.	Jason Jaworski	(electronic copy)
1	H3D Inc.	Christopher Wahl	(electronic copy)
1	Univ. of Michigan	Zhong He	(electronic copy)
1	Univ. of Michigan	Jiyang Chu	(electronic copy)
1	ORNL	Klaus Ziock	(electronic copy)
1	NSTEC	Rusty Trainham	(electronic copy)


Sandia National Laboratories